Applied Surface Science 255 (2009) 3795–3800

Contents lists available at ScienceDirect

Applied Surface Science

journal homepage: www.elsevier.com/locate/apsusc

$Pb(Zr_{0.53}Ti_{0.47})O_3$ thin films with different thicknesses obtained at low temperature by microwave irradiation

Ankam Bhaskar [a,*], Tsun-Hsu Chang [a], Horng-Yi Chang [b], Syh-Yuh Cheng [c]

[a] Department of Physics, National Tsing Hua University, Hsinchu 30013, Taiwan
[b] Department of Marine Engineering, National Taiwan Ocean University, Keelung 20224, Taiwan
[c] Material and Chemical Research Laboratories, Industrial Technology Research Institute, Hsinchu 31060, Taiwan

A R T I C L E I N F O

Article history:
Received 6 August 2008
Received in revised form 9 October 2008
Accepted 11 October 2008
Available online 1 November 2008

Keywords:
Microwave annealing
Surface roughness
Lead zirconate titanate
Leakage current

A B S T R A C T

$Pb(Zr_{0.53}Ti_{0.47})O_3$ (PZT) thin films with different thicknesses (99–420 nm) were prepared on Pt(1 1 1)/Ti/SiO_2/Si(1 0 0) substrates by sol–gel method and films were annealed at 450 °C for 30 min using a single-mode cavity of 2.45 GHz microwaves. X-ray diffraction analysis indicated that the pyrochlore phase was transformed to the perovskite phase at above 166 nm films. The grain sizes were increased, surface roughnesses were decreased, and electrical properties were improved with film thickness. The leakage current density was 9×10^{-8} A/cm^2 at an applied electrical field of 100 kV/cm. The ohmic and field-enhanced Schottky emission mechanisms were used to explain leakage current behavior of the PZT thin films. These results suggest that microwave annealing is effective for obtaining low temperature crystallization of thin films with better properties.

© 2008 Elsevier B.V. All rights reserved.

1. Introduction

The lead zirconate titanate ($Pb(Zr_xTi_{1-x})O_3$) (PZT) thin films $x = 0.53$ have different applications for their ferroelectric, piezoelectric, electro-optic, and pyroelectric properties [1,2]. Formation of the ferroelectric perovskite phase in PZT thin films generally requires a temperature of about 600 °C, which makes it difficult to integrate the thin films with silicon monolithic circuits. Therefore, reducing the processing temperature has been the goal for researchers. Many groups are attempting to prepare PZT thin films at low temperatures by various techniques such as electrophoretic deposition [3], hydrothermal synthesis [4], radio frequency sputtering [5], sol–gel process [6], CO_2 laser annealing [7], metal–organic chemical vapor deposition [8], and millimeter wave annealing [9].

The use of microwave energy for processing materials has recently become an attractive area for research [10–12]. The growing interest during the past decade is essentially due to the possibility of manufacturing cost reduction through energy savings, shorter processing times and improved product uniformity and yields. Microwave processing differs mainly in that the heat is generated within the material, instead of in an external heating source, a fact that is responsible for the unique microstructure and uniformity. Microwave processing has been used in annealing ferroelectric ceramic/films. Marques et al. [13] studied the crystallization of $CaTiO_3$ powder taking a very short time (30 min) using a domestic microwave oven, in contrast to 2 h required when using the conventional process at the same temperature. In addition, microwave sintered $CaTiO_3$ powders show higher structural organization and lower photoluminescent than that of conventionally sintered powders. Sharma et al. [14] studied the effect of 2.45 GHz microwaves on PZT ceramics using a multimode cavity, and compared it to the conventionally sintered PZT ceramics. They reported that microwave-sintered PZT ceramics has higher remanent polarization (P_r), and lower coercive field (E_c) than conventionally sintered PZT ceramics. Zanetti et al. [15] reported that the time required to crystallize $SrBi_2Ta_2O_9$ thin films thoroughly was drastically reduced (700 °C/10 min) when a domestic microwave oven was used, rather than a conventional furnace (700 °C/2 h). Vasconcelos et al. [16] reported that a domestic microwave oven (2.45 GHz) enhanced the crystallization of $SrBi_2Nb_2O_9$ (SBN) thin films at 700 °C for 30 min over the conventional annealed SBN thin films at 700 °C for 2 h. Mazon et al. [17] reported that the $Ba_{0.65}Sr_{0.35}TiO_3$ thin film yield creak-free, well-adhered, and fully crystallized with high dielectric constant (699) and low dielectric loss (0.018) at 100 kHz. Song et al. [18] completely formed a perovskite phase PZT thin film using the

* Corresponding author. Present address: Microwave Assisted Process Division, Green Technologies, Environmental Science and Technology Centre, Ottawa, ON, K1AOH3 Canada. Tel.: +1 613 993 6109; fax: +1 613 990 2855.
E-mail addresses: ankambhaskar@gmail.com, ankam.bhaskar@ec.gc.ca (A. Bhaskar).

0169-4332/$ – see front matter © 2008 Elsevier B.V. All rights reserved.
doi:10.1016/j.apsusc.2008.10.043

multimode cavity of 2.45 GHz microwaves at a lower temperature (600 °C) than required to form a conventionally annealed PZT thin film (700 °C). Its dielectric loss was lower, and the remnant polarization was higher than those of a conventionally annealed PZT thin film. However, low temperature processing (<500 °C) of PZT thin films with different thicknesses using 2.45 GHz microwaves has not been reported.

Recently, we have reported the effect of microwave annealing temperature on PZT thin films [19], and the comparison of microwave and conventional annealing of PZT thin films [20]. In this study, we have prepared PZT thin films with different thicknesses on Pt(1 1 1)/Ti/SiO_2/Si(1 0 0) substrate, then annealed at 450 °C for 30 min using a single-mode cavity of 2.45 GHz microwaves. The crystal structure, the surface morphology, and the electrical properties of PZT thin films were investigated. Based on the experimental results, the effect of thickness on PZT thin films was discussed.

2. Experimental

The PZT precursor solution was fully described elsewhere [19,20]. The precursor solution was deposited on Pt(1 1 1)/Ti/SiO_2/Si(1 0 0) substrates by spin coating at 500 rpm for 1 s and at 3000 rpm for 15 s. The as-deposited layer was dried on a hot plate in air at 150 °C for 5 min and decomposed at 400 °C for 10 min to evaporate alcohol and organics. The decomposition temperature was established by the thermogravimetric analysis [21], which indicates that at 400 °C, most of the organics are evaporated and decomposed from the PZT thin films. The spin coating and drying process were repeated up to 10 cycles layer by layer.

The PZT thin films were placed in a casket, which was thermally insulated. The casket was located at the center of the highest electric field in the applicator. SiC rods are used as susceptors because PZT does not absorb 2.45 GHz microwaves at room temperature [14]. The microwave energy initially heated the SiC rods, which, in turn, transferred heat to the insulation and eventually to the thin film [22]. As the temperature of the PZT thin film increased, it more effectively coupled with the microwave energy, promoting direct heating. Also, residuals organic compounds when pulverized generate amorphous carbon powders, which are able to absorb rapidly the microwave (2.45 GHz frequency) [23] and consequently to increase the temperature at approximately 1283 °C in just 1 min in a microwave irradiation system operating at 1 kW [24]. The temperature was measured using a thermocouple (Pt and 87%Pt–13%Rh) with an alumina sheath, which was in contact with the surface of the thin film. The PZT thin films were annealed by 2.45 GHz microwaves at 450 °C for 30 min.

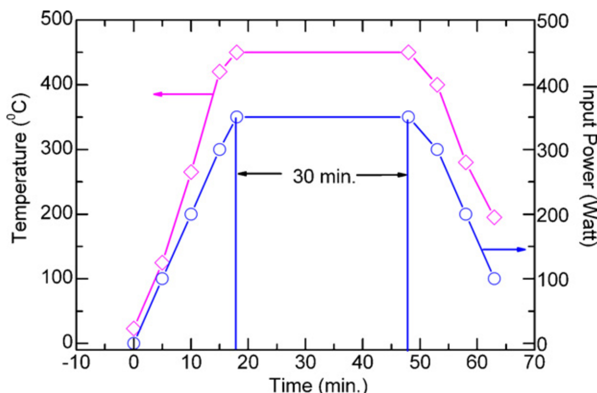

Fig. 1. Time vs. temperature and input power profile for the microwave annealing of PZT thin film.

The crystallization and the phase formation of all the annealed thin films were examined at room temperature with X-ray diffraction (XRD) system (Rigaku D/MAX-IIB at 40 kV and 30 mA), Cu Kα radiation wavelength λ = 1.5405 Å in the glazing angle (1°), every 0.02° between 2θ = 20° and 60°. The film thicknesses and surface morphologies of the PZT thin films were examined under field emission scanning electron microscope (FE-SEM) (JSM-6500F). The surface roughnesses of PZT thin films were characterized using a Seiko Instrument (Inc. SPI3800N) atomic

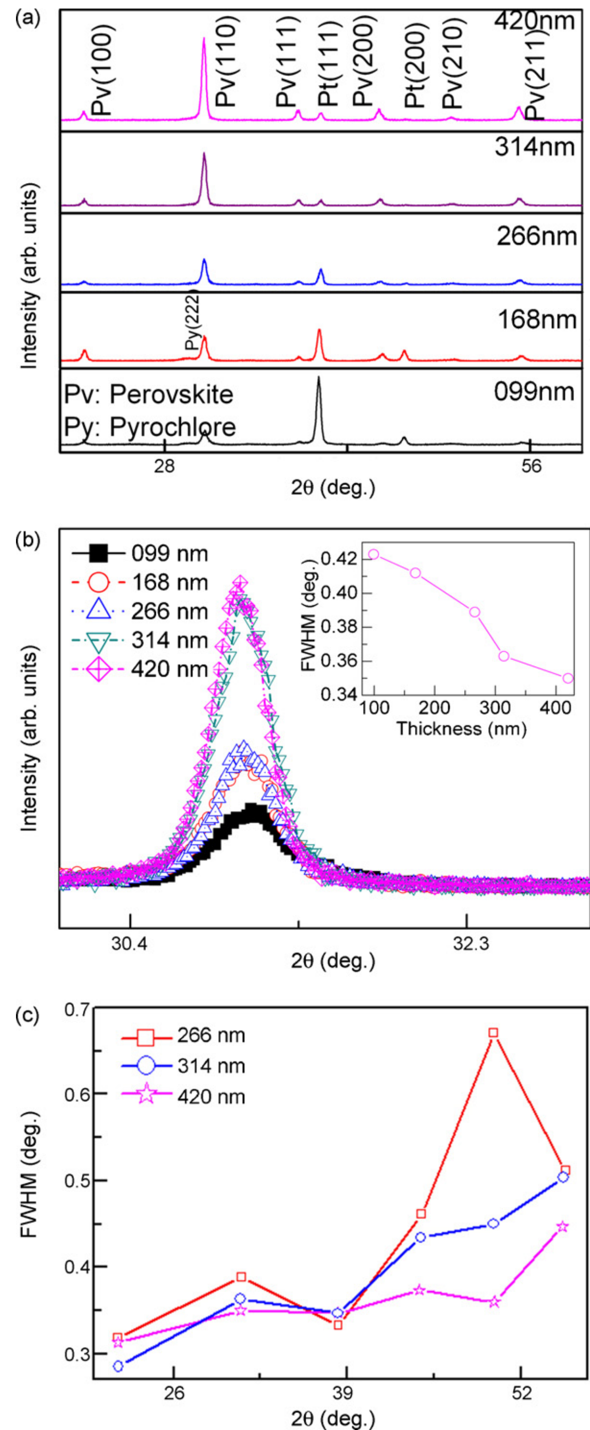

Fig. 2. (a) XRD pattern of PZT thin films with different thicknesses; (b) peak at 2θ = 30–33° observed in XRD pattern (a) redrawn in expanded scale to emphasize the different intensities of the perovskite phase peak (1 1 0) and FWHM; (c) all perovskite phase peak of FWHM.

force microscope (AFM) system. Au electrodes were deposited by rf sputtering on the top surface of PZT thin films through a shadow mask with a diameter of 1 mm for electrical measurements. This deposition was conducted at room temperature. The dielectric properties were measured at 1 kHz using an impedance analyzer (HP impedance/gain analyzer 4194A). The polarization–electric (*P–E*) hysteresis loops were measured using a Radiant Technologies RT-66A ferroelectric test system by applying triangular voltages at a frequency of 1 kHz. The current density–electric field (*J–E*) characteristic was measured by a computer controlled high-voltage source measurement unit (Keithley 2400).

3. Results and discussion

Fig. 1 shows the profiles of time versus temperature and input power. The microwave annealing was conducted at 450 °C for 30 min with an average ramp rate of 25 °C/min. Excluding the cooling period; it took about 48 min, which was shorter than the conventional annealing time (>1 h). It is worthy to note here that the input power (350 W) was much lower than those reported by Wang et al. [9] (2.5 kW) and Song et al. [18] (2 kW), and no hot spots were observed, a fact that usually occurs in microwave processing of materials due to the thermal runaway (unstable accelerated heating).

Fig. 2a shows the XRD patterns of PZT thin films annealed at 450 °C for 30 min with different thicknesses. The 99 nm and 168 nm PZT films exhibit the perovskite and pyrochlore phase peaks, indicating that the films were partially transformed from pyrochlore phase to perovskite phase. As the film thickness increased to 266 nm, the pyrochlore phase disappeared, and it was completely transformed to the perovskite phase. The 314 nm and 420 nm PZT films have complete perovskite structure. The peak with the highest intensity in the XRD patterns of the PZT thin films were indexed as (1 1 0) planes, indicating that the thin films were mostly randomly oriented, which agree with earlier reports [9,18]. Kwok and Desu [25] reported that whenever the second phase such as pyrochlore was formed, the pyrochlore to perovskite conversion occurs through an interface-controlled transformation by isotropic growth, and that the resultant films had a random orientation with a strong (1 1 0) PZT reflection. The full width at half maximum (FWHM) of the perovskite phase peak (1 1 0) was considered in evaluating the quality of the PZT thin films [26,27]. In all of the XRD patterns (Fig. 2a), a peak at around $2\theta = 30–33^{\circ}$ was observed corresponding to the (1 1 0) planes of the perovskite phase. This peak was redrawn on an expanded scale in Fig. 2b, and all perovskite phase peaks of FWHM were also shown in Fig. 2c. The 314 nm and 420 nm PZT films yield narrower FWHM of all perovskite phase peaks than the other annealed films, it suggests that these films have high perovskite contents. The perovskite phase peak (1 1 0) of the 420 nm PZT film was higher, and the FWHM (0.35°) was narrower than the other annealed films. These results confirm that the microwave annealing has a strong dependence on the film thickness [18].

We examined the surface morphologies of PZT thin films by field emission scanning electron microscope (FE-SEM). Fig. 3 shows the surface morphologies of PZT thin films with different thicknesses. The 168 nm PZT film yielded rosette structure which consisted of large (~1 μm) round shape grains [28,29]. The image of the region of the small grains was enlarged, clearly revealing dense grains (~16 nm). The 266 nm PZT film reveals the fine

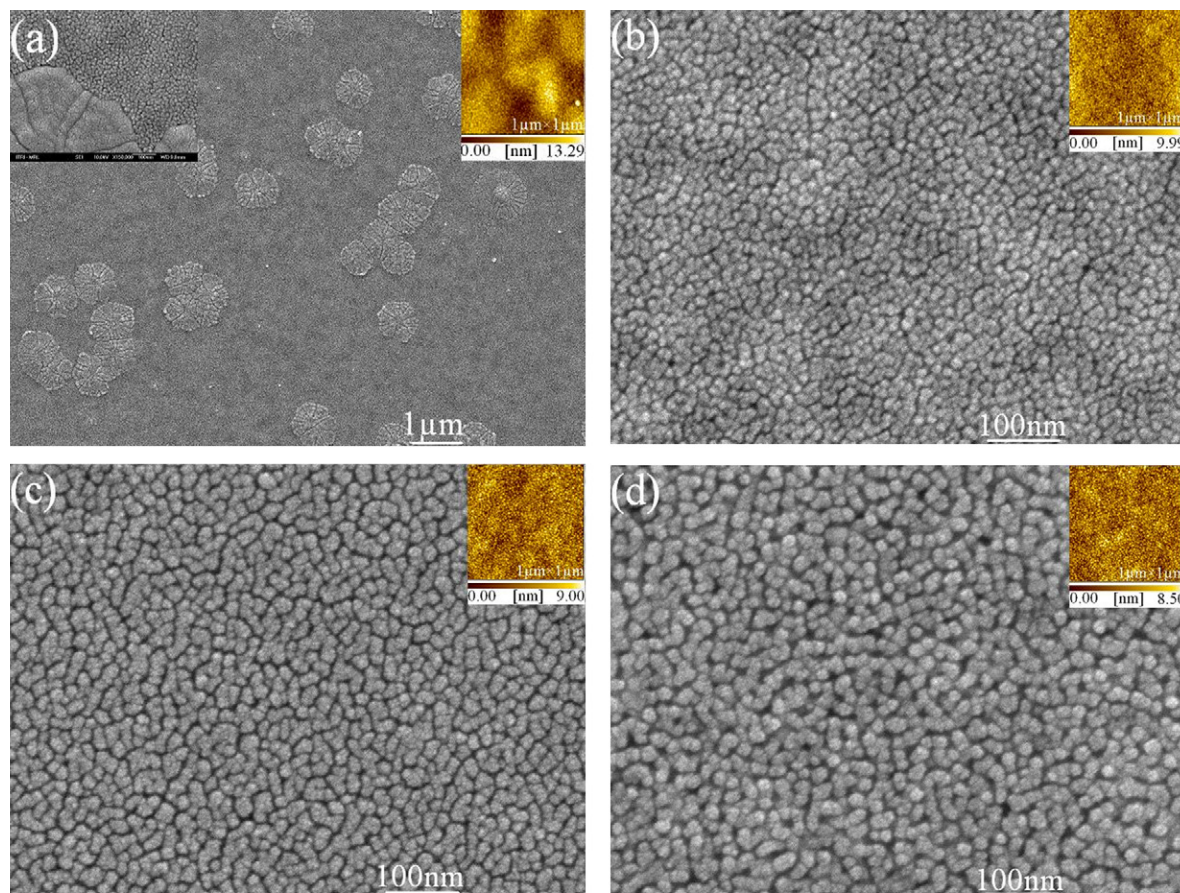

Fig. 3. FE-SEM images of PZT thin films with different thicknesses: (a) 168 nm, (b) 266 nm, (c) 314 nm and (d) 420 nm.

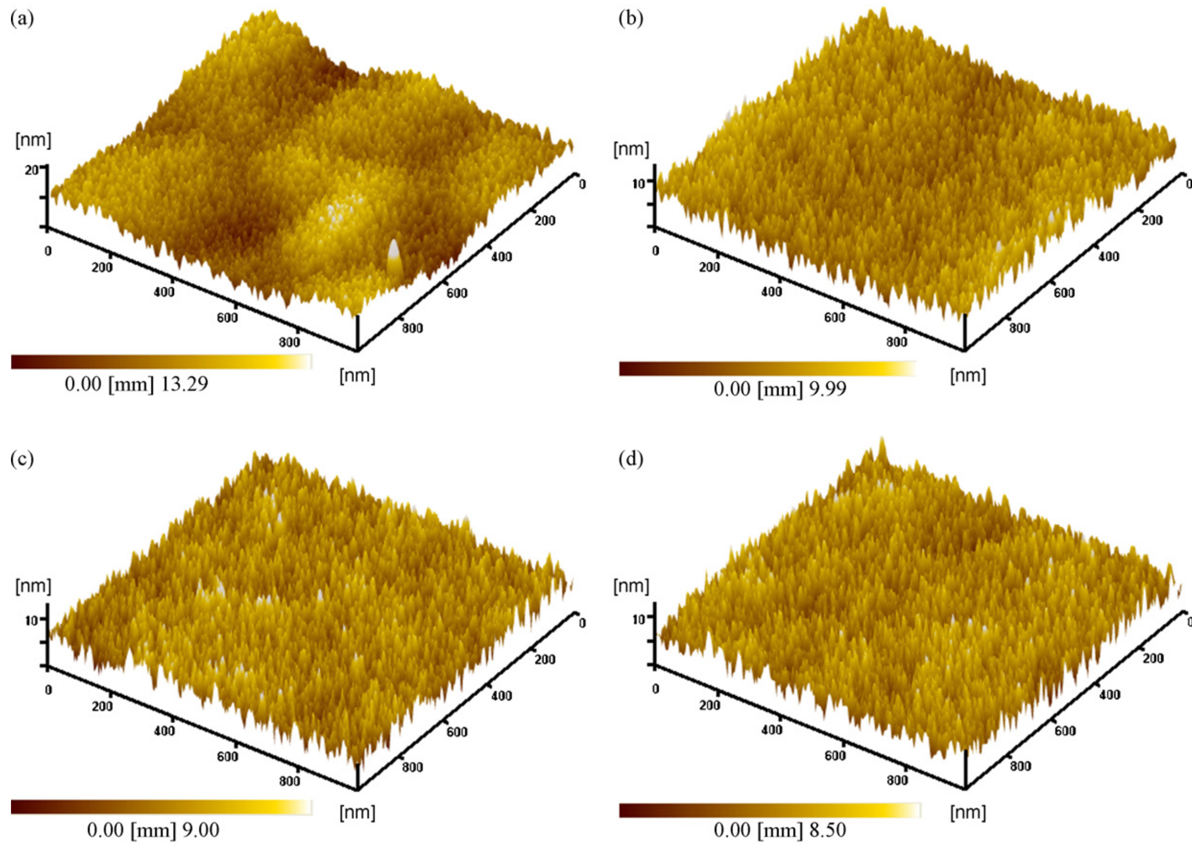

Fig. 4. The AFM three-dimensional images of PZT thin films: (a) 168 nm, (b) 266 nm, (c) 314 nm and (d) 420 nm.

grains, with an average grain size of (~22 nm) (Fig. 3a). The 312 nm PZT film was smooth and voide-free; the grains were well crystallized and homogeneously distributed, and had an average grain size of (~25 nm) (Fig. 3b). The 420 nm PZT film also yields dense and fine grains, with an average grain size of (~30 nm) (Fig. 3c). The grain sizes were increased with an increasing film thickness and were within the range of ~30 nm which is less than the conventionally annealed PZT thin films [9]. The ferroelectric perovskite phase generally forms in PZT thin films [30] at over 600 °C, but the microwave-annealed PZT thin films perovskite phase occurred at 450 °C with high perovskite content (Fig. 2). Therefore, the microwave annealing is more effective than the conventional annealing. The low temperature can be ascertained by smaller grains microstructure (Fig. 3) in comparison with the conventional process [9]. The intensity of the microwave field is at least three times higher in cavities [31,32], which are capable of rapidly heating the thin films with shorter processing time which might lead to the suppression of movement of grain boundaries [33]. Furthermore, the microwave driving force might be lowering down the Pb atoms therefore jumping energy the barrier to transform pyrochlore to the perovskite phase at this low annealing temperature (450 °C) [19]. However, further work must be performed to elucidate the details of the interaction between the microwaves and the PZT thin films (see coupling of TiO_2, PbO, Pt and ZrO_2 with microwave irradiation).

The surface roughnesses and the three-dimensional image of PZT thin films were also examined by AFM. Fig. 4 shows AFM (3D) surface images of PZT thin films with different thicknesses. The 168 nm PZT film yield crack-free surface and large grains embedded in a small-grain matrix with round shapes. A careful analysis of this image also suggested the presence of circular rosettes, which, in general, develops from their surrounding nanoscale pyrochlore matrix. In addition, the SEM morphology also yielded rosette structure (Fig. 3a). Similar rosette structure was reported for PZT thin films earlier [34–37]. The 99 nm and 168 nm PZT films yield hillocks which are due to the stress induced between the films and the substrate [38]. Also the substrate peak intensity was higher than other film peaks as indicated in XRD pattern (Fig. 2a). The 266 nm, 314 nm, and 420 nm PZT films yielded larger grains and were more uniformly distributed without the hillocks. Furthermore, the R_a and R_{rms} measured by AFM, R_a is the average roughness, and R_{rms} is the root means square roughness. Fig. 5 shows the roughness parameters (R_a, R_{rms}) with different thicknesses. As can be observed, the surface roughnesses of PZT thin films decreased as the film thickness increased. It is

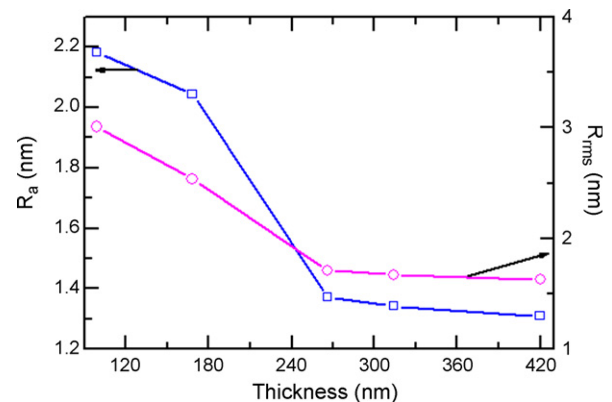

Fig. 5. Surface roughnesses of PZT thin films with different thicknesses.

Table 1
Comparison data (ε_r, D, P_r and E_c) of PZT thin films with various annealing methods.

PM	AM	Composition	AT (°C/min)	Thickness (μm)	ε_r (1 kHZ)	Loss (D)	P_r (μC/cm^2)	E_c (kV/cm)	Ref.
SG	CA	53/47	550/120	0.50	0700	0.05	41.0	115.0	[46]
SG	RTA	53/47	550/05	0.30	0850	0.05	32.2	079.9	[47]
SG	FA + LA	53/47	550/60	0.17	–	–	30.3	123.5	[48]
SG	HP	52/48	600/30	0.70	0900	0.05	15.0	045.0	[49]
SG	CO_2LA	52/48	–	0.37	–	–	17.3	039.8	[7]
SG Input: 2.5 kW	MI	52/48	480	1.00	1100	0.04	40.0	050.0	[9]
SG Input: 2 kW	MA	50/50	600/06	0.45	0500	0.03	08.4	047.5	[18]
SG Input: 350 W	MA	53/47	450/30	0.42	1140	0.03	46.86	086.25	Present work

PM: preparation method; AM: annealing method; AT: annealing temperature; SG: sol–gel; CA: conventional annealing; RTA: rapid thermal annealing; FA + LA: furnace + laser annealing; HP: hybrid process (sol–gel + pulse-laser deposition); LA: laser annealing; MI: microwave irradiation (28 GHz); MA: microwave annealing (2.45 GHz).

expected that the grain size increases and the surface morphology becomes smoother when the film thickness increases. These results are in agreement with those reported by others [39]. The changes surface microstructure observed with film thickness are due to the changes in the crystallinity and the decrease in stress.

The cross-sectional FE-SEM image reveals the PZT thin films with multilayer (PZT, Pt, Ti, SiO_2, and Si) structures as well as the interface between the PZT film and the bottom electrode (Pt). Each layer exhibits very dense, uniform, sharp interfaces between the film and the electrode [19,20]. The thicknesses of PZT thin films were found approximately 99, 168, 266, 314, and 420 nm respectively.

The dielectric constant (ε_r) was increased and the dissipation factor (D) was decreased with film thickness (314 nm film: ε_r, 673; D, 0.055; and 420 nm film: ε_r, 1140; D, 0.03), respectively [19,20]. The remnant polarization was increased and coercive field was decreased with film thickness (314 nm film: P_r, 39.38 μC/cm^2; E_c, 116.50 kV/cm; and 420 nm film: P_r, 46.86 μC/cm^2; E_c, 86.25 kV/cm), respectively [19,20]. It is well known that the use of a template/buffer layer with a good mismatch in lattice and structure can promote the perovskite formation [40,41], but in our case, the thin films exhibit good electrical properties without buffer/template layer which are usually a big challenge for technological applications such as microelectronic and micro-system developments.

Table 1 presents the data for processing the PZT thin films with various annealing methods and compares them to the present PZT thin films data. Among the various annealing methods, the present microwave annealed PZT thin films exhibit higher dielectric constant, lower dissipation factor, and higher remnant polarization, and moderate coercive field than the literature data [7,9,18,46–49].

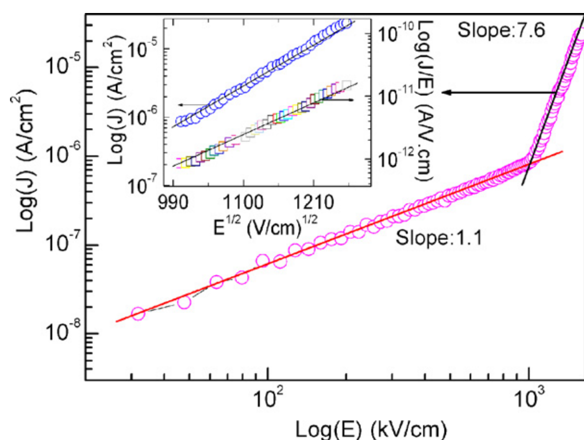

Fig. 6. Leakage current characteristic of the 420 nm PZT thin film. The inset in figure: $\log_{10}(J)$ and $\log_{10}(J/E)$ vs. $E^{1/2}$ plots.

One of the most important features for a material to be used as an alternative for functional applications is the low leakage current density. Fig. 6 shows the positively bias leakage current data in the form of the $\log_{10}(J)$ vs. $\log_{10}(E)$. It can be seen that there are two clearly different regions, i.e., the low electric field (<1000 kV/cm) and the high electric field region (>1000 kV/cm). In the low electric field region, the slope of the $\log_{10}(J)$ vs. $\log_{10}(E)$ curve was 1.1, indicating that the current in the low electric field region was ohmic-like. In the high electric field region, the slope of the $\log_{10}(J)$ vs. $\log_{10}(E)$ curve was 7.6, implying that the conduction mechanism has been changed. The current density was a function of the square root of the electrical field (as shown in the inset of the figure). The conduction mechanisms were normally ascribed either the Poole–Frenkel (bulk-like mechanism (PF)) or the field-enhanced Schottky emission (interface-controlled mechanism (ES)) at higher electrical field. The conduction mechanism could be distinguished on the basis of the extracted dynamic dielectric constant from the ES or PF. The dynamic dielectric constant extracted from the slope of the $\log_{10}(J/E)$ vs. $E^{1/2}$ curve, using the PF mechanism, was 32.86. On the other hand, by fitting the slope of the $\log_{10}(J)$ vs. $E^{1/2}$ curve for ES mechanism, the dynamic dielectric constant was extracted to be 6.17 using ES mechanism. The dynamic dielectric constant extracted from ES is very close to the optical dielectric constant [42] (ε_r: 6.76), while that from the PF is not. It is likely that the mechanism is ES conduction. Similar I–V curves of conventionally annealed PZT thin films have been previously reported [43,44]. The leakage current density (10^{-8} A/cm^2) was almost three orders of magnitude lower than the hybrid process [45] (10^{-5} A/cm^2) at the same electrical field of 75 kV/cm. This was the first experimental characterization of the leakage current for microwave irradiation annealed PZT thin films.

4. Conclusion

Using the 2.45 GHz microwave annealing, it is possible to obtain PZT thin films with high perovskite content at low temperature (450 °C). The thin films exhibit dense, well-crystallized microstructure having random orientation with a dominant (1 1 0) reflection. The electrical properties were improved with film thickness such as P_r of 46.86 μC/cm^2, E_c of 86.25 kV/cm, ε_r of 1140, respectively. The J–E characteristics yield two kinds of mechanisms that are Ohmic and field-enhanced Schottky emission mechanisms. The electrical properties were comparable with those of other methods, and it can be concluded that the microwave annealing method is useful for low temperature crystallization of thin films.

Acknowledgements

The authors would like to thank the Industrial Technology Research Institute (ITRI) of the Republic of China, Taiwan, for financially supporting this research under Contract No. ITRI 94C03. Professor K.R. Chu of the Department of Physics at the National Tsing Hua University is acknowledged for his technical support.

References

[1] J.F. Scott, C.A.P. Arajuo, Science 246 (1989) 1400.
[2] D. Damjanovic, Rep. Prog. Phys. 61 (1998) 1267.
[3] S. Sugiyama, A. Takagi, K. Tsuzuki, Jpn. J. Appl. Phys. 30 (1991) 2170.
[4] T. Morita, Y. Wagastsuma, Y. Cho, H. Morioka, H. Funakubo, N. Setter, Appl. Phys. Lett. 84 (2004) 5094.
[5] S. Watanabe, T. Fujiu, T. Fujii, Appl. Phys. Lett. 66 (1995) 1481.
[6] Y.J. Song, Y. Zhu, S.B. Desu, Appl. Phys. Lett. 72 (1998) 2686.
[7] H.C. Pan, C.C. Chou, H.L. Tsai, Appl. Phys. Lett. 83 (2003) 3156.
[8] J.W. Moon, S. Tazawa, K. Shinozaki, N. Wakiya, N. Mizutani, Appl. Phys. Lett. 89 (2006) 202907.
[9] Z.J. Wang, H. Kokawa, H. Takizawa, M. Ichiki, R. Maeda, Appl. Phys. Lett. 86 (2005) 212903.
[10] W.H. Sutton, Am. Ceram. Soc. Bull. 68 (1989) 376.
[11] R. Roy, D. Agrawal, J. Cheng, S. Gedevanishvili, Nature 399 (1999) 668.
[12] Z. Cao, Z. Wang, N. Yoshikawa, S. Taniguchi, J. Phys. D: Appl. Phys. 41 (2008) 092003.
[13] V.S. Marques, L.S. Cavalcante, J.C. Sczancoski, D.P. Volanti, J.W.M. Espinosa, M.R. Joya, M.R.M.C. Santos, P.S. Pizani, J.A. Varela, E. Longo, Solid State Sci. 10 (2008) 1056.
[14] P.K. Sharma, Z. Ounaies, V.V. Vardan, V.K. Varadan, Smart Mater. Struct. 10 (2001) 878.
[15] S.M. Zanetti, J.S. Vasconcelos, N.S.L.S. Vasconcelos, E.R. Leite, E. Longo, J.A. Varela, Thin Solid Films 466 (2004) 62.
[16] J.S. Vasconcelos, N.S.L.S. Vasconcelos, S.M. Zanetti, E.R. Leite, J.A. Varela, E. Longo, Appl. Surf. Sci. 225 (2004) 156.
[17] T. Mazon, M.A. Zaghete, J.A. Varela, E. Longo, J. Eur. Ceram. Soc. 27 (2007) 3799.
[18] S. Song, X. Fu, H. Tan, M. Tao, L. Chen, L. Wang, C. Lin, Phys. Status Sol. A 164 (1997) 779.
[19] A. Bhaskar, H.Y. Chang, T.H. Chang, S.Y. Cheng, Nanotechnology 18 (2007) 395704.
[20] A. Bhaskar, T.H. Chang, H.Y. Chang, S.Y. Cheng, Thin Solid Films 515 (2007 2891).
[21] F.M. Pontes, E.R. Leite, M.S.J. Nunes, D.S.L. Pontes, E. Longo, R. Magnani, P.S. Pizani, J.A. Varela, J. Eur. Ceram. Soc. 24 (2004) 2969.
[22] N.S.L.S. Vasconcelos, J.S. Vasconcelos, V. Bouquet, S.M. Zanetti, E.R. Leite, E. Longo, L.E.B. Soledade, F.M. Pontes, M. Guilloux-Viry, A. Perrin, M.I. Bernardi, J.A. Varela, Thin Solid Films 436 (2003) 213.
[23] L.S. Cavalcante, V.S. Marques, J.C. Sczancoski, M.T. Escote, M.R. Joya, J.A. Varela, M.R.M.C. Santos, P.S. Pizani, E. Longo, Chem. Eng. J. 143 (2008) 299.
[24] K.J. Rao, B. Vaidhyanathan, M. Ganguli, P.A. Ramakrishnan, Chem. Mater. 11 (1999) 882.
[25] C.K. Kwok, S.B. Desu, Ceram. Trans. 25 (1992) 82.
[26] C.C. Chang, Y.C. Lai, J. Appl. Phys. 101 (2007) 104106.
[27] I. Bretos, J. Ricote, R. Jimenez, J. Mendiola, R.J. Jimenez Rioboo, M.J. Calzada, J. Eur. Ceram. Soc. 25 (2005) 2325.
[28] C.H. Wang, D.J. Choi, J. Am. Ceram. Soc. 84 (2001) 207.
[29] C.D.E. Lakeman, D.A. Payne, J. Am. Ceram. Soc. 75 (1992) 3091.
[30] C.K. Kwok, S.B. Desu, Appl. Phys. Lett. 60 (1992) 1430.
[31] A. Birnbiom, J.P. Calame, Y. Carmel, J. Appl. Phys. 85 (1999) 478.
[32] J.P. Calame, K. Rybakov, Y. Carmel, D. Gershon, Microwave: theory and application in materials processing IV, in: D.E. Clark, W.H. Sutton, D.A. Lewis (Eds.), Ceram. Trans., vol. 80, The American Ceramic Society, Ohio, 1997, p. 135.
[33] G.F. Xu, I.K. Lloyd, Y. Camel, T. Olorunyoleni, O.C. Wilson, J. Mater. Res. 16 (2001) 2850.
[34] M.T. Escote, F.M. Pontes, E.R. Leite, E. Longo, R.F. Jardim, P.S. Pizani, J. Appl. Phys. 96 (2004) 2186.
[35] R. Thomas, S. Mochizuki, T. Mihara, T. Ishida, Jpn. J. Appl. Phys. 40 (2001) 5511.
[36] W. Zhu, Z.Q. Liu, M.S. Tse, H.S. Tan, X. Yao, J. Appl. Phys. 79 (1996) 4283.
[37] M. Mandeljc, B. Malic, M. Kosec, Integr. Ferroelectr. 52 (2003) 205.
[38] S. Baba, K. Numata, H. Saito, M. Kumagai, T. Ueno, B. Kyoh, S. Miyake, Thin Solid Films 390 (2001) 70.
[39] H. Maiwa, N. Ichinose, Jpn. J. Appl. Phys. 42 (2003) 4392.
[40] K. Ishikawa, K. Sakura, D. Fu, S. Yamada, Jpn. J. Appl. Phys. 37 (1998) 5128.
[41] E. Cattan, G. Velu, B. Jaber, D. Remiens, B. Thierry, Appl. Phys. Lett. 70 (1997) 1718.
[42] G. Yi, Z. Wu, M. Sayer, J. Appl. Phys. 64 (1988) 2717.
[43] T. Mihara, H. Watanabe, Jpn. J. Appl. Phys. 34 (1995) 5664.
[44] T. Mihara, H. Watanabe, Jpn. J. Appl. Phys. 34 (1995) 5674.
[45] Z.J. Wang, H. Kokawa, R. Maeda, M. Ichiki, Jpn. J. Appl. Phys. 43 (2004) 6554.
[46] H. Suzuki, T. Koizumi, Y. Kondo, S. Kaneko, J. Eur. Ceram. Soc. 19 (1999) 1397.
[47] X.G. Tang, L.L. Jiang, A.L. Ding, Microelectron. Eng. 65 (2003) 387.
[48] Y. Zhu, J. Zhu, Y.J. Song, S.B. Desu, Appl. Phys. Lett. 73 (1998) 1958.
[49] Z.J. Wang, H. Kokawa, R. Maeda, Acta Mater. 53 (2005) 593.